Tandem Mass-selective Cryogenic Digital Ion Traps for Enhanced Cluster Formation

Gina C. Roesch[a] and Etienne Garand[a*]

[a]Department of Chemistry, University of Wisconsin-Madison, 1101 University Ave, Madison, Wisconsin 53706, United States

*Corresponding Author Email:

egarand@wisc.edu (E.G.)

Abstract

We present the implementation of tandem mass-selective cryogenic ion traps, designed to enhance the range of ion processing capabilities that can be performed prior to spectroscopic interrogation. We show that both the formation of ion clusters and mass filtering steps can be combined in a single cryogenic linear quadrupole ion trap driven by RF square waves. Mass filtering and mass isolation can be achieved by manipulation of the RF frequency and duty cycle. Very importantly, this scheme circumvents the need for high-amplitude RF voltages that can be incompatible with typical cryogenic ion processing conditions. In addition, proper adjustment of the stability boundaries during the clustering process allows for the preferential formation of a specific cluster size rather than a broad distribution of sizes. Lastly, we show that a specific cluster size can be formed, mass-selected, and then transferred to another ion trap for a second, completely separate ion processing step. The instrumentation and modular design developed here expands the scope of ionic species and clusters that can be accessed by processing electrosprayed ions.

I. Introduction

Cryogenic ion vibrational spectroscopy (CIVS) combines mass spectrometry with laser infrared spectroscopy to reveal structural information on mass-selected ions of interest. Its operation relies on using cryogenic ion traps to cool ions via collisions with buffer gas and condense onto the ions a small, minimally-perturbative "tag" atom/molecule whose laser-induced loss is the crux of vibrational action spectroscopy.[1–3] Condensation of the tag onto the mass-selected ions requires a trap temperature of 8-30 K (typically 10 K for H_2/D_2 tags), which imposes a significant limit on the composition of the buffer gas and the possibility of processing the ions in any other way. A few years ago, we introduced a dual cryogenic ion trap instrument[4] aimed at overcoming this limitation while maintaining the ability to efficiently form tagged adducts. The instrument involves using a separate variable temperature (80-300 K) ion trap to process the ions produced by electrospray ionization (ESI). These ions are then transferred to the tagging (10 K) ion trap for tag adduct formation and subsequent spectroscopic interrogation. Within each of these two tandem ion traps, buffer gas composition, pressure, and temperature can be varied independently to optimize the conditions for each step. Examples of ion processing that can be carried out in the first trap include transformation via temperature-controlled ion−molecule reactions and condensation of solvent molecules to form ionic clusters.[5] This approach has been used to study catalytic reaction intermediates[6,7] and microsolvated ions.[8–17]

However, having only one ion processing step before tagging limits the complexity of the accessible species. Some example applications of multiple ion processing steps include forming a species from ion-molecule reaction and then condensing solvent molecules onto it or exposing it to another reagent to probe reactivity; forming clusters comprising two different solvent molecules or depositing a different species on the surface of a microsolvated cluster; and adding a pre-thermalizing step for the reactant prior to temperature-dependent ion-molecule kinetics studies.

The obvious approach here is to increase the number of ion processing traps. However, the lack of mass-selectivity prior to each trapping stage can lead to interferences from unwanted species produced by either the ESI or the prior ion processing step. And this issue is compounded with each additional ion trap. Moreover, any solvent condensation processing would typically yield a large distribution of cluster sizes such that any specific desired size is found with much

lower intensity than the initial parent ion. This is particularly detrimental when trying to access larger clusters that can only be produced in very broad size distributions.[4]

The removal of unwanted species can be accomplished by incorporating mass filtering steps in the ion manipulation sequence. For example, quadrupole mass filters are commonly used prior to injection into a cryogenic trap.[14,18–23] However, such filters suffer from poor transmission efficiency, particularly at higher m/z.[24–28] Here, we present a novel approach that uses mass-selective cryogenic linear quadrupole ion traps that combine ion processing and filtering capabilities. This approach provides additional flexibility by allowing specific mass-selective conditions to be applied at any time during the trapping cycle. In particular, we show that by using proper mass-selective conditions during the clustering process, we can selectively enhance the formation of a specific cluster size.

There are limited examples of mass-selective cryogenic ion traps in the literature.[29,30] The main challenges in implementing such technology for ion processing traps lies in the need for relatively high buffer gas pressure and the inevitable condensation of solvent or reactant molecules onto the cold trap assembly, both of which are incompatible with the application of high amplitude RF voltages necessary in conventional approaches to quadrupole mass filtering. To circumvent this issue, our cryogenic quadrupole ion processing traps are driven with square waves (sometimes referred to as digital waves) instead of the more common sine waves. Square wave driven mass selective devices typically utilize variable RF frequency and duty cycle at fixed low-amplitude RF voltages for mass analysis.[31–36] While the use of square waves to drive mass selective devices was described more than 50 years ago,[31] it recently gained more traction in the mass spectrometry community mostly as a way to access larger mass ranges.[32,34,35,37–41] For the purposes outlined here, the use of square waves additionally has the advantages of lower costs and ease of fabrication, needing only relatively simple frequency generators and MOSFET based high-voltage switches. This, in conjunction with the modular design presented here, offers the possibility of implementing several ion processing mass-selective traps in tandem to prepare ever more complex and interesting chemical species for spectroscopic interrogation.

II. Methods

a) Prototype modular instrument

The results presented in this paper are acquired using a prototype instrument, shown schematically in Figure 1. It consists of a simple ESI source, two linear quadrupole cryogenic ion traps and a short linear time-of-flight (TOF) detector. Ions are formed by electrospraying a millimolar solution of peptides in methanol through a 30 µm tip silica emitter, and they entered the mechanically-pumped stage (~4 Torr) via a 10 cm long 0.76 mm ID stainless-steel capillary tube. The ions then crossed into the subsequent differentially-pumped stage (~400 mTorr) via a 0.9 mm aperture skimmer. From here, the ions are transferred via two RF-only hexapole ion guides driven by an RF oscillator based on the design of O'Connor[42,43] into the first ion trap. The region housing the first ion trap is held at ~1x10^{-4} Torr by a ~300 L/s turbomolecular pump.

The design of the cryogenic linear ion trap is nearly identical to our initial report,[4] except the linear octupole geometry is replaced with a quadrupole arrangement to allow for mass filtering.[44,45] The ion trap, whose details are shown in Figure 2C, is composed of two copper blocks, each holding two round stainless-steel rods. The rods are 19.8 mm in diameter and 9.5 mm long and are placed within the copper housing such that the inscribed radius, r_0, is 4.2 mm. The copper blocks are spaced by a PEEK insulator to create a trap volume, which is enclosed on both ends by a 3.8 mm copper aperture. The entrance aperture is typically held <1V above the

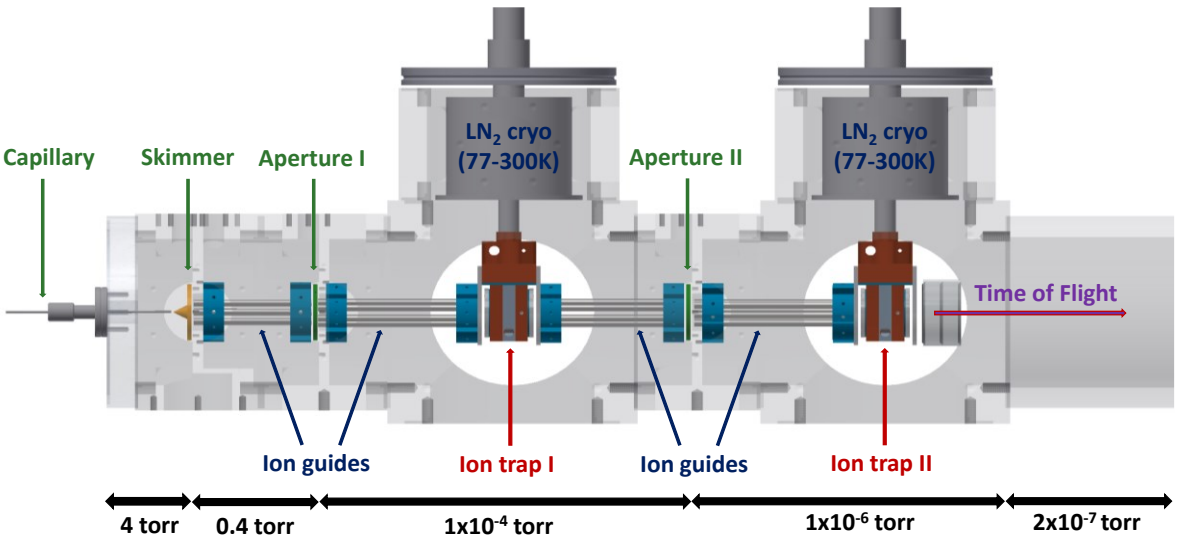

Figure 1. Schematic of the tandem mass-selective cryogenic digital ion trap prototype instrument

quadrupole rod bias. The exit aperture is held ~10V above the rod bias when loading and processing the ions. It is switched to ~5-15V below the rod bias to extract the ions from the trap and transfer them to the next stage. A miniature solenoid valve (Parker Series 25), connected to

the internal trap volume via a ~3 cm long Teflon tube is used to pulse in helium buffer gas seeded with the desired solvent vapor to initiate cooling and formation of clusters.

The ion trap is attached to a home-built variable temperature (80-300 K) liquid-nitrogen cryostat whose temperature is monitored by a Pt RTD sensor and adjusted using a 50 W heating cartridge. All the electrical feedthroughs for the ion trap are located on an aluminum collar with the cryostat flange such that the entire assembly can easily be taken out of the vacuum chamber for cleaning and maintenance. The ion trap assembly is housed in a cubic aluminum chamber with an ISO100 port on each face, a modular and versatile design in which an additional ion trap can easily be inserted or removed from the instrument. The cubic chambers are connected to one another via spacer blocks that hold the ion guides and apertures. These spacer blocks also have ports for an aperture, ion guide electrical feedthroughs and a cold cathode vacuum gauge.

In our prototype instrument, after the first ion trap, the ions are transferred into another differentially pumped region (~$1x10^{-6}$ Torr) with a second identical ion trap via two hexapole ion guides and an aperture. The second ion trap is followed by a short co-linear TOF detector region (~$2x10^{-7}$ Torr) for acquiring mass spectra. We note that the co-linear ion-trap/TOF geometry resulted in a rather modest mass resolution due to the wide spread of ion velocities from the linear ion trap extraction. However, it is sufficient for demonstrating the capabilities of the prototype instrument.

b) Square wave RF generator and driver

Each quadrupole ion trap is driven by fixed amplitude $150V_{p-p}$ RF square waves with variable frequency and duty cycle. The square waves are generated using a low voltage waveform generator and a pair of high-voltage bipolar MOSFET switches, as shown schematically in Figure 2A. The waveform generator is based on the design of Hoffmann, *et. al.*[46,47] and is composed of an Arduino DUE microcontroller that controls one direct digital synthesis (DDS) module and two digital-to-analog converters (DACs). The DDS module generates a 5V sine wave with the desired frequency that is then fed into two linear comparators. The DACs set a reference DC voltage that each comparator uses to create two opposite-phase 5V square waves with the desired duty cycles. Here, duty cycle (d) is defined as the amount of time that the square wave spends at the high voltage (t) relative to one full period (T) of the waveform, as shown in Figure 2B. The duty cycle for the X and Y rods are adjusted separately for controlling the oscillations of the trapped ions and

the resulting stability zones.[33,34,48–52] Therefore, we will refer to the duty cycle in the format of d_x:d_y. For example, a duty cycle of 55:55 represents square waves that are high for 55% of the period for both X and Y rods. Each opposite-phase low voltage waveform is used to control an individual half-bridge MOSFET bipolar switch. The outputs are switched between the positive

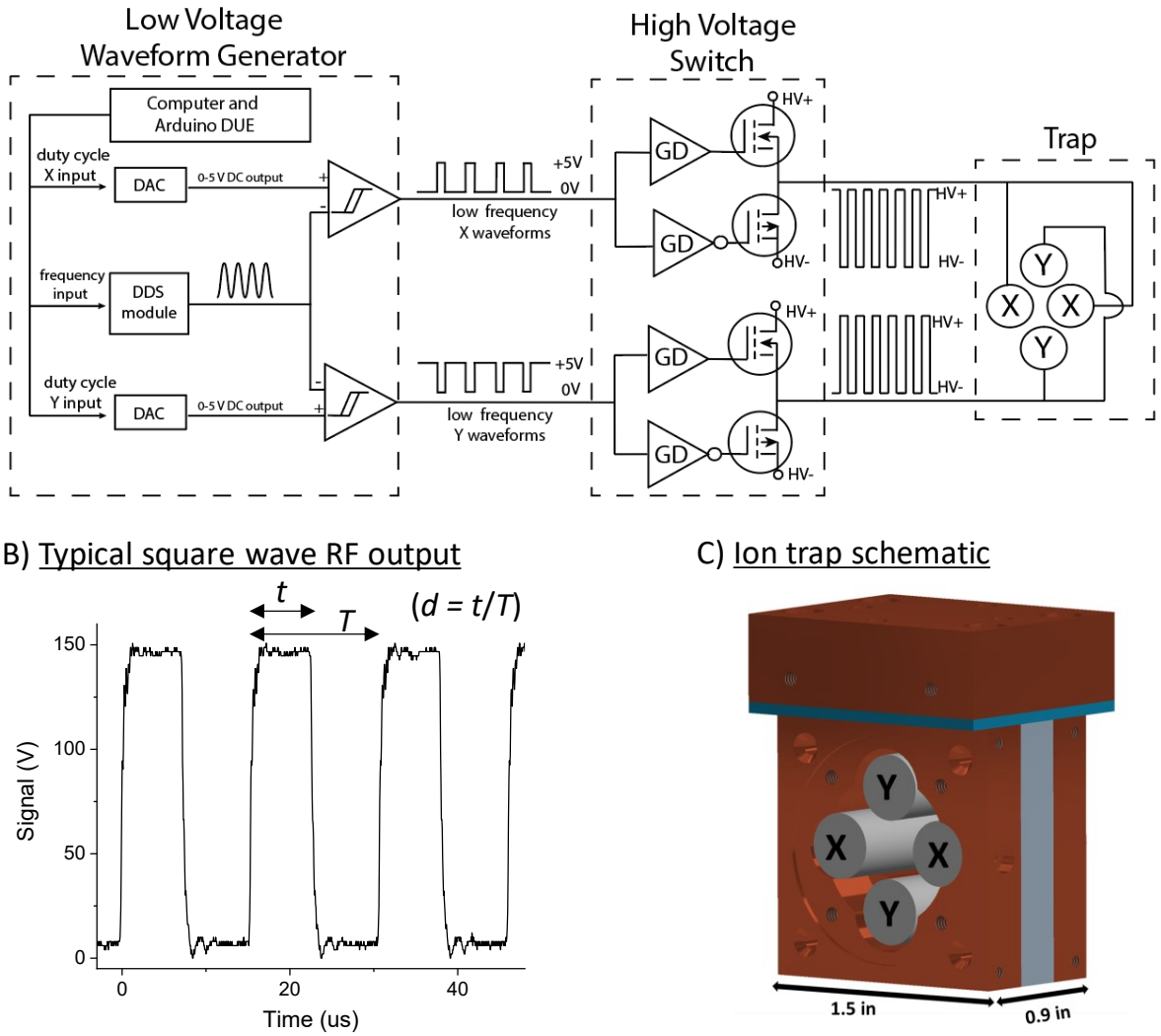

Figure 2. A) Schematic of the square wave RF generator; B) Typical output with f = 650 kHz and d = 50 from the generator. The definition of the duty cycle is shown here in relation to the output trace; C) Schematic of the linear quadrupole ion trap.

and negative floating outputs of a 3W, 150VDC power supply and create the X and Y rods' driving square waves. Both X and Y rods are floated with the same DC voltage to create an overall ion trap bias. Overall, this driver allows for square waves with frequency up to 650 kHz, a limit imposed by the power requirement and heat dissipation of the current bipolar switches design.

III. Results and Discussion

a) Clustering in square wave quadrupole ion trap

We begin by demonstrating that the square driving wave and steeper effective potential of the quadrupole ion trap geometry[53] do not interfere with the ability to perform clustering operations. Figure 3 shows the mass spectra obtained when protonated trialanine peptide (Ala_3H^+, m/z = 232) is produced by ESI and processed only in the second ion trap. In these experiments, the second ion trap is held at 80 K and the helium buffer gas pulsed into the trap is seeded with water vapor. The RF frequencies are maintained at 650 kHz with 50:50 duty cycle for the entire trapping cycle. The presence of a peak progression separated by 18 m/z in the mass spectra shows that $Ala_3H^+(H_2O)_n$ clusters are readily formed under these conditions. Increasing the gas pulse amplitude resulted in the formation of larger clusters, similar to our previous report[4] that used an octupole ion trap driven with ~800 kHz sine waves.

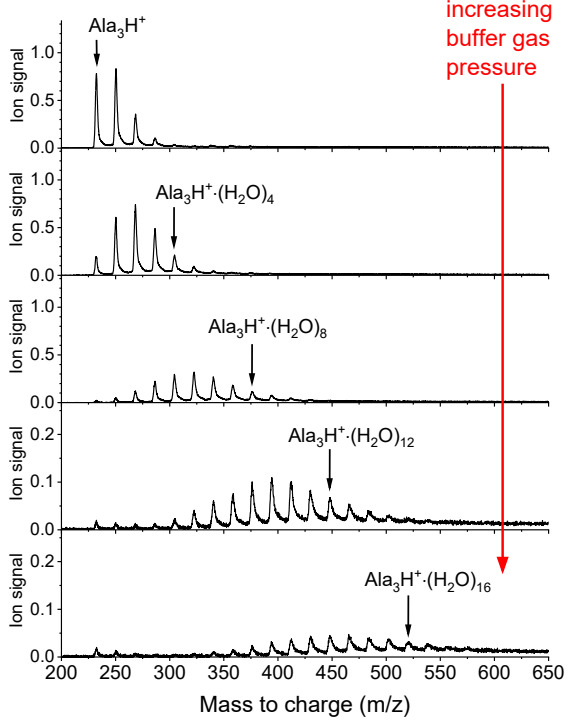

Figure 3. Formation of $Ala_3H^+\cdot(H_2O)_n$ clusters by condensation of water molecules onto the Ala_3H^+ ion in the 80 K cryogenic ion trap as a function of the buffer gas pressure. Note the different vertical scale of the last two panels.

Figure 3 also illustrates the issue of low signal intensity encountered when producing larger clusters with $n > 10$. As the buffer gas pressure is increased to access the larger clusters, the wider distribution yields very little signal for each individual cluster size. Moreover, the total ion signal tends to decrease at higher buffer gas pressures due to ion losses under these conditions.

Finally, we varied the length of the trapping cycle and found that most of the clusters are formed within the first 1 ms following the initiation of the gas pulse. This result likely reflects the kinetics of water condensing onto trap walls and poles at 80 K, and points to possible future modifications that can improve the clustering process. For example, if we can introduce solvent vapor and buffer gas separately, we may be able to lengthen

the cluster formation time window without increasing the overall pressure inside the ion trap thereby promoting formation and preservation of the larger clusters.

b) Mass filtering with frequency and duty cycle manipulation

One of the reasons for using square waves is that we would be able to perform the clustering process and mass-filtering step within a single trapping cycle. Mass filtering with square waves can be accomplished by changing the frequency and duty cycle of the driving RF. The stability diagram for square wave quadrupoles[31,37,48,49] can be derived using matrix solutions of the Mathieu equations and can be defined in terms of the commonly used a and q dimensionless Mathieu parameters:

$$a = \frac{8zeU}{mr_0^2\omega^2} \qquad q = \frac{4zeV}{mr_0^2\omega^2}$$

Here, m and ze are the mass and the charge of the ion, r_0 is the inscribed radius of the quadrupole, $\omega = 2\pi f$ is the angular frequency, and V is the amplitude of the alternating potential. The U variable is the DC offset between the X and Y rods. In our implementation, the square waves driving both X and Y rods come from the same power supply, and hence there is no DC offset, and $a = 0$.

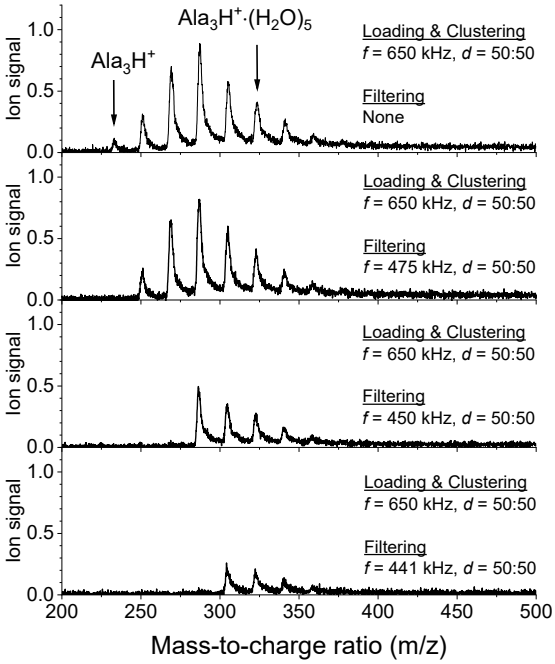

Figure 4. Formation of a $Ala_3H^+\cdot(H_2O)_n$ cluster distribution and subsequent high-pass m/z filtering by lowering the trap RF frequency for 200 μs after the clustering process.

The square wave stability diagram has a first stability region in the a,q space that is of similar shape but shifted relative to the sine-wave case.[31,37,48,52] For the simplest case of a 50:50 square wave and $a = 0$, ions with $q < 0.7125$ have a stable trajectory inside the ion trap. This critical q value defines the smallest m/z ion with a stable trajectory for a given set of V, r_0 and f. Therefore, by changing the frequency we can change the smallest stable m/z,

effectively creating a high-pass filter. This is illustrated in Figure 4. The top panel shows the mass spectrum without filtering, obtained by keeping the square wave at f = 650 kHz and 50:50 duty cycle for the entire 22 ms trapping cycle. The trap conditions are set such that a $Ala_3H^+\cdot(H_2O)_n$ cluster distribution peaking around n = 3 is maintained. Keeping all else the same, a high-pass filtering step can be inserted towards the end of the trapping cycle by lowering the RF frequency for the last 200 μs. For example, when the frequency is lowered to f = 475 kHz, the Ala_3H^+ parent at m/z=232 is removed and when lowered to f = 450 kHz or f = 441 kHz, clusters smaller than $Ala_3H^+\cdot(H_2O)_3$ or $Ala_3H^+\cdot(H_2O)_4$ are filtered out, respectively.

The effect of changing the duty cycle is less trivial to understand. In general, increasing the duty cycle has a somewhat similar effect as increasing the DC offset, and thus yields a smaller range of stable q values. Therefore, increasing d_x:d_y while keeping ω constant can be used to effectively create a low-pass filter. This is illustrated in Figure 5. Again, the top panel shows the mass spectrum without filtering, obtained with f = 650 kHz and d_x:d_y = 50:50 for the entire trapping cycle. In the bottom three panels, the frequency is kept constant while the duty cycle is changed during the last 200 μs of the trapping cycle. These mass spectra show how increasing from 50:50 to 54.35:54.65 can eliminate all the clusters larger than $Ala_3H^+\cdot(H_2O)_5$, and increasing to 55.1:55.5 or 56.0:56.5 eliminated cluster size larger than $Ala_3H^+\cdot(H_2O)_3$ or $Ala_3H^+\cdot(H_2O)_1$, respectively.

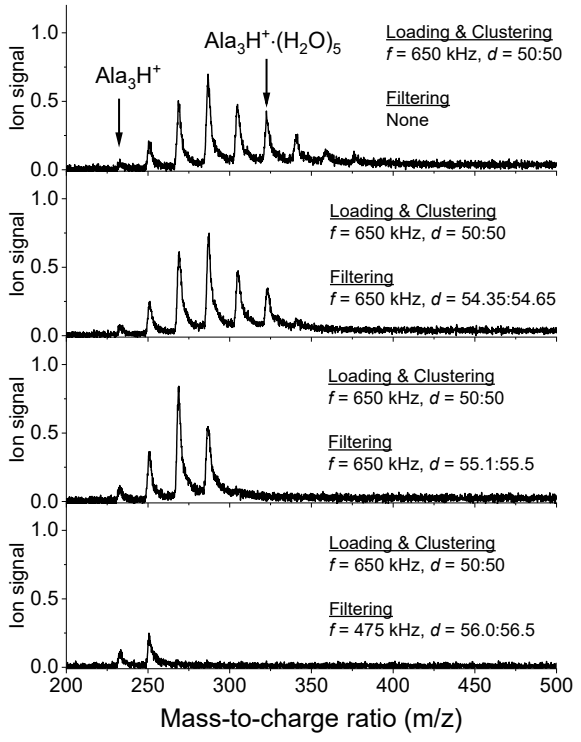

Figure 5. Formation of a $Ala_3H^+\cdot(H_2O)_n$ cluster distribution and subsequent low-pass m/z filtering by increasing the square wave duty cycle for 200 us after the clustering process.

Thus, combining frequency and duty cycle manipulations can isolate a specific cluster size. In principle, both can be applied simultaneously by choosing the right combination of frequency and duty cycle to bring the desired mass near the apex of the stability region. However, the effect of the duty cycle is frequency dependent, which complicates

determining the exact combination necessary for mass isolation. A simpler approach is to apply the high-pass and low-pass filtering conditions (determined from Figures 4 and 5) sequentially, and there is ample time within each trapping cycle to perform both operations. Figure 6 illustrates this process by selectively isolating $Ala_3H^+\cdot(H_2O)_2$, $Ala_3H^+\cdot(H_2O)_3$ or $Ala_3H^+\cdot(H_2O)_4$ species. For each trapping cycle, RF square waves are first held at 650 kHz and 50:50 to load the parent ions in the trap and condense solvent onto them. Then, d_x:d_y is increased to create a low-pass filter for 1.5 ms, eliminating all clusters larger than the desired size. After which, the RF wave is returned to 650 kHz and 50:50 for 10 ms. During the last 1 ms of the cycle, the frequency is lowered to eliminate all clusters smaller than the desired size. Note that the high-pass filter must be placed at the very end of the trapping cycle to remove the parent ions, which are continuously injected into the trap during the cycle.

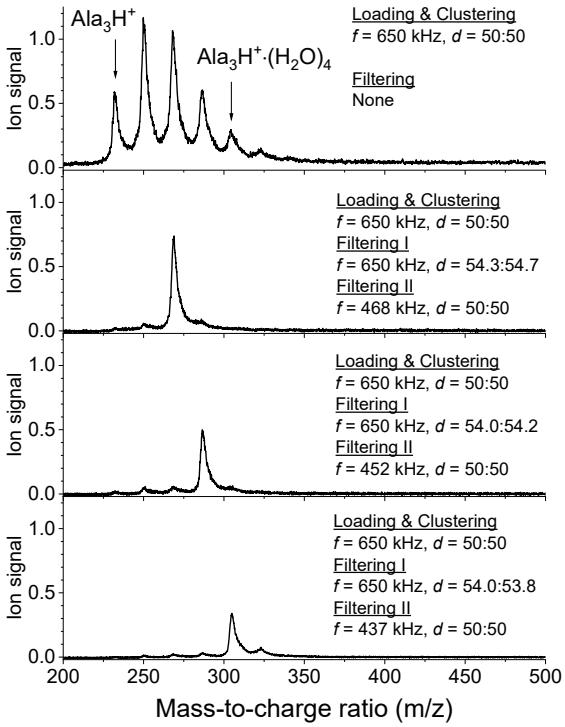

Figure 6. Formation of a $Ala_3H^+\cdot(H_2O)_n$ cluster distribution and subsequent mass isolation by sequential low-pass and high-pass filtering steps after the clustering process.

Figure 6 shows that clusters separated by 18 m/z can be isolated with minimal loss. For mass isolation using the apex of the stability diagram, isolation of smaller m/z ranges always comes at the expense of some loss of the desired mass. In our experiment, the mass-resolution in the isolation step may be additionally limited by the short length of the ion trap, which results in quadrupolar field distortions from the end caps. A more efficient mass isolation scheme would involve the use of auxiliary dipolar excitation,[54,55] as commonly found in mass-selective ion trap setups.

c) Clustering step manipulation and enhancement

Instead of manipulating the duty cycle after the cluster formation time window, we can do so during clustering to enhance the formation of a particular cluster size. Specifically, d_x:d_y can

be set such that the parent ion is well within the stability region, but as water molecules are added, the cluster eventually reaches the boundary of the stability region. This leads to excitation of ion motions and energetic collisions with the buffer gas, which then rapidly leads to fragmentation and loss of a water molecule. Once the cluster mass is reduced, it finds itself back in the stability region and its motion would be cooled by the buffer gas. Overall, this process can prevent the growth of cluster sizes past a certain point and effectively accumulate the largest cluster size that is within the stability region.

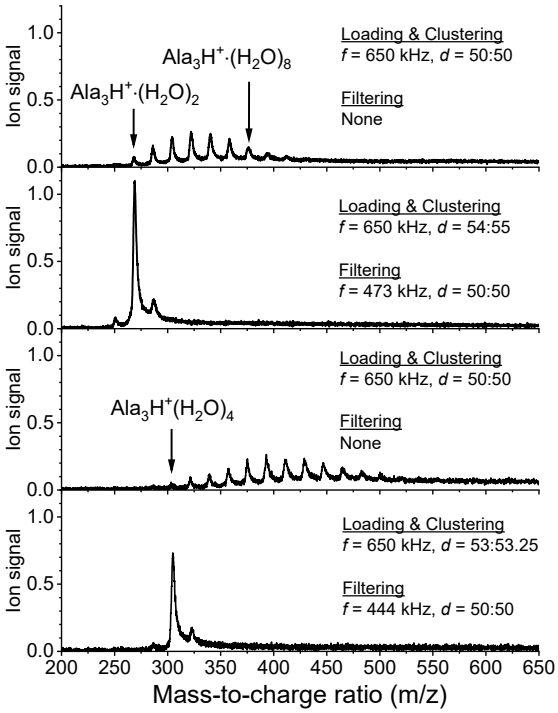

Figure 7. Enhanced formation and isolation of specific $Ala_3H^+\cdot(H_2O)_n$ cluster sizes by increasing the duty cycle during the clustering process and subsequent application of a high-pass m/z filter.

The result of this process is illustrated in Figure 7. The top panel shows the cluster distribution obtained without any filtering. The second panel shows the result of applying a duty cycle of 54:55, corresponding to $Ala_3H^+\cdot(H_2O)_2$ being the largest cluster accumulated, for 1 ms at the start of the trapping cycle (i.e., the entire time of cluster formation). At the end of the cycle, the frequency is decreased to eliminate any remaining parent or smaller clusters. This resulted in $Ala_3H^+\cdot(H_2O)_2$ intensity which is significantly (~25 times) larger than in the original distribution. A similar process is shown in the two bottom panels in Figure 7 for the enhanced formation of the $Ala_3H^+\cdot(H_2O)_4$ species. Note that the best enhancements are obtained under the conditions where most of the original distribution is larger than the desired cluster size. The intensity of the enhanced cluster size is ~75% of the total intensities of the larger clusters in the original distribution, indicating that some ion losses are occurring during the process. Finally, we note that fragmentation was not observed when d_x:d_y is raised after the initial 1 ms. This is likely due to the lower pressure inside the trap after the buffer gas pulse is mostly evacuated, and hence the excitation of ion motions mainly result in ion loss and not fragmentation.

d) Transfer and second clustering step

Having demonstrated the capabilities of a single digital ion trap, we now show how multiple ion traps can be combined to perform sequential ion processing. The top panel of Figure 8 shows the initial $Ala_3H^+\cdot(H_2O)_n$ cluster distribution created in the first ion trap. The $Ala_3H^+\cdot(H_2O)_2$ cluster is then selectively enhanced using the duty cycle and frequency manipulations described in the previous section, and the resulting ions are transferred into the second ion trap. The mass distribution obtained after trapping and holding the $Ala_3H^+\cdot(H_2O)_2$ cluster ions in the second ion trap for 30 ms is shown in the second panel of Figure 8. Successful ion transfer requires careful adjustment of the buffer gas pulse timing in the second trap to match the ion packet's arrival time, similar to the operation of our previously reported dual trap spectrometer.[4] Moreover, the second trap's bias voltage needs to be kept within ~1 V of that of the first trap to minimize ion kinetic energy and facilitate trapping. Higher ion kinetic energy can result in fragmentation and loss of water molecules from the clusters.

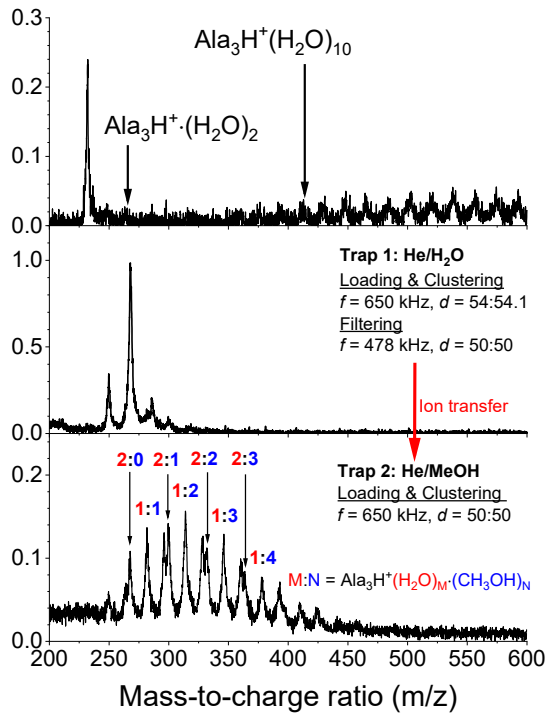

Figure 8. Tandem operation in which the $Ala_3H^+\cdot(H_2O)_2$ cluster is selectively formed in the first ion trap and transferred into the second ion trap where methanol clustering is performed.

A second clustering processing step is demonstrated by seeding the buffer gas of the second ion trap with methanol vapor. The resulting cluster distribution, shown in the bottom panel of Figure 8, consisted mostly of $Ala_3H^+\cdot(H_2O)_1\cdot(CH_3OH)_N$ and $Ala_3H^+\cdot(H_2O)_2\cdot(CH_3OH)_N$ clusters. The $Ala_3H^+\cdot(CH_3OH)_N$ species are also present to a smaller extent. This result indicates that a significant fraction of the initial $Ala_3H^+\cdot(H_2O)_2$ clusters undergo fragmentation during the second clustering step. This is likely due to the increased buffer gas pressure required to carry out clustering. Better results may be achievable by separating the gas pulses required for the initial ion trapping/translational cooling from the

introduction of the solvent vapor necessary for clustering. Nevertheless, this result demonstrates how combination of both ion traps and the use of selective enhancement in the first trap can yield an overall small distribution of clusters containing two different solvent molecules.

IV. Conclusions

We present here the implementation of a modular tandem mass-selective cryogenic ion trap setup designed to expand ion processing capabilities in experiments such as CIVS. We showed that both clustering and mass filtering steps can be combined into a single mass-selective ion trap that is driven by variable frequency and duty cycle RF square waves. Mass filtering and mass isolation are achieved by proper manipulation of the RF frequency and duty cycle, which avoid the need for high-amplitude RF voltages. Moreover, adjustment of the stability boundary during the clustering process allows for preferential formation of a specific cluster size rather than a broad distribution of sizes. Lastly, we show that a specific cluster size can be formed, mass-selected, and then transferred to a second ion trap for a separate ion processing step. The instrumentation developed here, together with future improvements, hold the promise of significantly expanding the scope of ionic species and clusters that can be accessed by processing electrosprayed ions.

Acknowledgements

Part of this work related to multistep ion processing was supported by the National Science Foundation under Grant No. CHE-1954268. The ion solvation part of this work was supported by the US Department of Energy, Office of Science, Basic Energy Sciences, under award no. DE-SC0018902

References

(1) Wolk, A. B.; Leavitt, C. M.; Garand, E.; Johnson, M. A. Cryogenic Ion Chemistry and Spectroscopy. *Acc. Chem. Res.* **2014**, *47* (1), 202–210. https://doi.org/10.1021/ar400125a.

(2) Kamrath, M. Z.; Garand, E.; Jordan, P. A.; Leavitt, C. M.; Wolk, A. B.; Van Stipdonk, M. J.; Miller, S. J.; Johnson, M. A. Vibrational Characterization of Simple Peptides Using Cryogenic Infrared Photodissociation of H-2-Tagged, Mass-Selected Ions. *J. Am. Chem. Soc.* **2011**, *133* (16), 6440–6448. https://doi.org/10.1021/ja200849g.

(3) Kamrath, M. Z.; Relph, R. A.; Guasco, T. L.; Leavitt, C. M.; Johnson, M. A. Vibrational Predissociation Spectroscopy of the H2-Tagged Mono- and Dicarboxylate Anions of Dodecanedioic Acid. *Int. J. Mass Spectrom.* **2011**, *300* (2–3), 91–98. https://doi.org/10.1016/j.ijms.2010.10.021.

(4) Marsh, B. M.; Voss, J. M.; Garand, E. A Dual Cryogenic Ion Trap Spectrometer for the Formation and Characterization of Solvated Ionic Clusters. *J. Chem. Phys.* **2015**, *143* (20), 204201. https://doi.org/10.1063/1.4936360.

(5) Garand, E. Spectroscopy of Reactive Complexes and Solvated Clusters: A Bottom-Up Approach Using Cryogenic Ion Traps. *J. Phys. Chem. A* **2018**, *122* (32), 6479–6490. https://doi.org/10.1021/acs.jpca.8b05712.

(6) Duffy, E. M.; Marsh, B. M.; Voss, J. M.; Garand, E. Characterization of the Oxygen Binding Motif in a Ruthenium Water Oxidation Catalyst by Vibrational Spectroscopy. *Angew. Chem.-Int. Ed.* **2016**, *55* (12), 4079–4082. https://doi.org/10.1002/anie.201600350.

(7) Craig, S.; Menges, F.; Johnson, M. Application of Gas Phase Cryogenic Vibrational Spectroscopy to Characterize the CO2, CO, N-2 and N2O Interactions with the Open Coordination Site on a Ni(I) Macrocycle Using Dual Cryogenic Ion Traps. *J. Mol. Spectrosc.* **2017**, *332*, 117–123. https://doi.org/10.1016/j.jms.2016.11.015.

(8) Fischer, K. C.; Sherman, S. L.; Voss, J. M.; Zhou, J.; Garand, E. Microsolvation Structures of Protonated Glycine and L-Alanine. *J. Phys. Chem. A* **2019**, *123* (15), 3355–3366. https://doi.org/10.1021/acs.jpca.9b01578.

(9) Voss, J. M.; Fischer, K. C.; Garand, E. Accessing the Vibrational Signatures of Amino Acid Ions Embedded in Water Clusters. *J. Phys. Chem. Lett.* **2018**, *9* (9), 2246–2250. https://doi.org/10.1021/acs.jpclett.8b00738.

(10) Voss, J. M.; Marsh, B. M.; Zhou, J.; Garand, E. Interaction between Ionic Liquid Cation and Water: Infrared Predissociation Study of Bmim (+)Center Dot(H2O)(n) Clusters. *Phys. Chem. Chem. Phys.* **2016**, *18* (28), 18905–18913. https://doi.org/10.1039/c6cp02730j.

(11) Fischer, K. C.; Sherman, S. L.; Garand, E. Competition between Solvation and Intramolecular Hydrogen-Bonding in Microsolvated Protonated Glycine and Beta-Alanine. *J. Phys. Chem. A* **2020**, *124* (8), 1593–1602. https://doi.org/10.1021/acs.jpca.9b11977.

(12) Fischer, K. C.; Voss, J. M.; Zhou, J.; Garand, E. Probing Solvation-Induced Structural Changes in Conformationally Flexible Peptides: IR Spectroscopy of Gly(3)H(+)Center Dot(H2O). *J. Phys. Chem. A* **2018**, *122* (41), 8213–8221. https://doi.org/10.1021/acs.jpca.8b07546.

(13) Akasaka, K.; Hirata, K.; Haddad, F.; Dopfer, O.; Ishiuchi, S.; Fujii, M. Hydration-Induced Protomer Switching in p-Aminobenzoic Acid Studied by Cold Double Ion Trap Infrared Spectroscopy. *Phys. Chem. Chem. Phys.* **2023**, *25* (6), 4481–4488. https://doi.org/10.1039/d2cp04497h.

(14) Suzuki, Y.; Hirata, K.; Lisy, J. M.; Ishiuchi, S.; Fujii, M. Double Ion Trap Laser Spectroscopy of Alkali Metal Ion Complexes with a Partial Peptide of the Selectivity Filter in K+ Channels - Temperature Effect and Barrier for Conformational Conversions, 2021, *125*, 9609–9618. https://doi.org/10.1021/acs.jpca.1c06440.

(15) Suzuki, Y.; Hirata, K.; Lisy, J.; Ishiuchi, S.; Fujii, M. A Bottom-up Approach to the Ion Recognition Mechanism of K+ Channels from Laser Spectroscopy of Hydrated Partial Peptide-Alkali Metal Ion

Complexes. *Phys. Chem. Chem. Phys.* **2022**, *24* (35), 20803–20812. https://doi.org/10.1039/d2cp01667b.
(16) Suzuki, Y.; Hirata, K.; Lisy, J.; Ishiuchi, S.; Fujii, M. Double Ion Trap Laser Spectroscopy of Alkali Metal Ion Complexes with a Partial Peptide of the Selectivity Filter in K+ Channels-Temperature Effect and Barrier for Conformational Conversions. *J. Phys. Chem. A* **2021**, *125* (44), 9609–9618. https://doi.org/10.1021/acs.jpca.1c06440.
(17) Zviagin, A.; Yamaletdinov, R.; Nagornova, N.; Dömer, M.; Boyarkin, O. V. Revealing the Structure of Tryptophan in Microhydrated Complexes by Cold Ion Spectroscopy. *J. Phys. Chem. Lett.* **2023**, 6037–6042. https://doi.org/10.1021/acs.jpclett.3c01239.
(18) Buntine, J.; Carrascosa, E.; Bull, J.; Jacovella, U.; Cotter, M.; Watkins, P.; Liu, C.; Scholz, M.; Adamson, B.; Marlton, S.; Bieske, E. An Ion Mobility Mass Spectrometer Coupled with a Cryogenic Ion Trap for Recording Electronic Spectra of Charged, Isomer-Selected Clusters. *Rev. Sci. Instrum.* **2022**, *93* (4). https://doi.org/10.1063/5.0085680.
(19) Ishiuchi, S.; Wako, H.; Kato, D.; Fujii, M. High-Cooling-Efficiency Cryogenic Quadrupole Ion Trap and UV-UV Hole Burning Spectroscopy of Protonated Tyrosine. *J. Mol. Spectrosc.* **2017**, *332*, 45–51. https://doi.org/10.1016/j.jms.2016.10.011.
(20) Redwine, J.; Davis, Z.; Burke, N.; Oglesbee, R.; McLuckey, S.; Zwier, T. A Novel Ion Trap Based Tandem Mass Spectrometer for the Spectroscopic Study of Cold Gas Phase Polyatomic Ions. *Int. J. MASS Spectrom.* **2013**, *348*, 9–14. https://doi.org/10.1016/j.ijms.2013.04.002.
(21) Stearns, J. A.; Seaiby, C.; Boyarkin, O. V.; Rizzo, T. R. Spectroscopy and Conformational Preferences of Gas-Phase Helices. *Phys. Chem. Chem. Phys.* **2009**, *11* (1), 125–132. https://doi.org/10.1039/b814143f.
(22) Goebbert, D. J.; Wende, T.; Bergmann, R.; Meijer, G.; Asmis, K. R. Messenger-Tagging Electrosprayed Ions: Vibrational Spectroscopy of Suberate Dianions. *J. Phys. Chem. A* **2009**, *113* (20), 5874–5880. https://doi.org/10.1021/jp809390x.
(23) Gulyuz, K.; Stedwell, C.; Wang, D.; Polfer, N. Hybrid Quadrupole Mass Filter/Quadrupole Ion Trap/Time-of-Flight-Mass Spectrometer for Infrared Multiple Photon Dissociation Spectroscopy of Mass-Selected Ions. *Rev. Sci. Instrum.* **2011**, *82* (5), 054101. https://doi.org/10.1063/1.3585982.
(24) Ehlert, T. Determination of Transmission Characteristics in Mass Filters. *J. Phys. E-Sci. Instrum.* **1970**, *3* (3), 237-. https://doi.org/10.1088/0022-3735/3/3/418.
(25) Gibson, J.; Taylor, S. Prediction of Quadrupole Mass Filter Performance for Hyperbolic and Circular Cross Section Electrodes. *RAPID Commun. MASS Spectrom.* **2000**, *14* (18), 1669–1673. https://doi.org/10.1002/1097-0231(20000930)14:18<1669::AID-RCM80>3.3.CO;2-R.
(26) Huntley, A. P.; Brabeck, G. F.; Reilly, P. T. A. Influence of the RF Drive Potential on the Acceptance Behavior of Pure Quadrupole Mass Filters Operated in Stability Zones A and B. *Int. J. Mass Spectrom.* **2020**, *450* (116303). https://doi.org/10.1016/j.ijms.2020.116303.
(27) McIntosh, B.; Hunter, K. Influence of Realistic Fringing Fields on the Acceptance of a Quadrupole Mass Filter. *Int. J. MASS Spectrom. ION Process.* **1989**, *87* (2), 165–179. https://doi.org/10.1016/0168-1176(89)80020-5.
(28) Joseph, M.; McIntosh, D.; Gibson, J.; Taylor, S. Effects of the Source Gap on Transmission Efficiency of a Quadrupole Mass Spectrometer. *RAPID Commun. MASS Spectrom.* **2018**, *32* (9), 677–685. https://doi.org/10.1002/rcm.8094.
(29) Cismesia, A.; Tesler, L.; Bell, M.; Bailey, L.; Polfer, N. Infrared Ion Spectroscopy inside a Mass-Selective Cryogenic 2D Linear Ion Trap. *J. MASS Spectrom.* **2017**, *52* (11), 720–727. https://doi.org/10.1002/jms.3975.
(30) Tesler, L.; Cismesia, A.; Bell, M.; Bailey, L.; Polfer, N. Operation and Performance of a Mass-Selective Cryogenic Linear Ion Trap. *J. Am. Soc. MASS Spectrom.* **2018**, *29* (11), 2115–2124. https://doi.org/10.1007/s13361-018-2026-7.

(31) Richards, J. A.; Huey, R. M.; Hiller, J. A New Operating Mode for the Quadrupole Mass Filter. *Int. J. Mass Spectrom. Ion Phys.* **1973**, *12*, 317–339.
(32) Ding, L.; Sudakov, M.; Brancia, F.; Giles, R.; Kumashiro, S. A Digital Ion Trap Mass Spectrometer Coupled with Atmospheric Pressure Ion Sources. *J. MASS Spectrom.* **2004**, *39* (5), 471–484. https://doi.org/10.1002/jms.637.
(33) Berton, A.; Traldi, P.; Ding, L.; Brancia, F. L. Mapping the Stability Diagram of a Digital Ion Trap (DIT) Mass Spectrometer Varying the Duty Cycle of the Trapping Rectangular Waveform. *J. Am. Soc. Mass Spectrom.* **2008**, *19* (4), 620–625. https://doi.org/10.1016/j.jasms.2007.12.012.
(34) Singh, R.; Jayaram, V.; Reilly, P. Duty Cycle-Based Isolation in Linear Quadrupole Ion Traps. *Int. J. MASS Spectrom.* **2013**, *343*, 45–49. https://doi.org/10.1016/j.ijms.2013.02.012.
(35) McCabe, J.; Jones, B.; Walker, T.; Schrader, R.; Huntley, A.; Lyu, J.; Hoffman, N.; Anderson, G.; Reilly, P.; Laganowsky, A.; Wysocki, V.; Russell, D. Implementing Digital-Waveform Technology for Extended m/z Range Operation on a Native Dual-Quadrupole FT-IM-Orbitrap Mass Spectrometer. *J. Am. Soc. MASS Spectrom.* **2021**, *32* (12), 2812–2820. https://doi.org/10.1021/jasms.1c00245.
(36) Brancia, F. L.; McCullough, B.; Entwistle, A.; Grossman, J. G.; Ding, L. Digital Asymmetric Waveform Isolation (DAWI) in a Digital Linear Ion Trap, 2010, *21*, 1530–1533. https://doi.org/10.1016/j.jasms.2010.05.003.
(37) Ding, L.; Kumashiro, S. Ion Motion in the Rectangular Wave Quadrupole Field and Digital Operation Mode of a Quadrupole Ion Trap Mass Spectrometer. *Rapid Commun. Mass Spectrom.* **2006**, *20* (1), 3–8. https://doi.org/10.1002/rcm.2253.
(38) Reilly, P.; Chakravorty, S.; Bailey, C.; Obe, F.; Huntley, A. Will the Digital Mass Filter Be the Next High-Resolution High-Mass Analyzer? *J. Am. Soc. MASS Spectrom.* **2021**, *32* (10), 2615–2620. https://doi.org/10.1021/jasms.1c00234.
(39) Schrader, R.; Walker, T.; Chakravorty, S.; Anderson, G.; Reilly, P.; Russell, D. Optimization of a Digital Mass Filter for the Isolation of Intact Protein Complexes in Stability Zone 1,1. *Anal. Chem.* **2023**, *95* (5), 3062–3068. https://doi.org/10.1021/acs.analchem.2c05221.
(40) Reece, M. E.; Huntley, A. P.; Moon, A. M.; Reilly, P. T. A. Digital Mass Analysis in a Linear Ion Trap without Auxiliary Waveforms. *J. Am. Soc. Mass Spectrom.* **2020**, *31* (1), 103–108. https://doi.org/10.1021/jasms.9b00012.
(41) Lee, J.; Marino, M.; Koizumi, H.; Reilly, P. Simulation of Duty Cycle-Based Trapping and Ejection of Massive Ions Using Linear Digital Quadrupoles: The Enabling Technology for High Resolution Time-of-Flight Mass Spectrometry in the Ultra High Mass Range. *Int. J. MASS Spectrom.* **2011**, *304* (1), 36–40. https://doi.org/10.1016/j.ijms.2011.03.011.
(42) O'Connor, P.; Costello, C.; Earle, W. A High Voltage RF Oscillator for Driving Multipole Ion Guides. *J. Am. Soc. MASS Spectrom.* **2002**, *13* (12), 1370–1375. https://doi.org/10.1016/S1044-0305(02)00700-6.
(43) Mathur, R.; O'Connor, P. Design and Implementation of a High Power Rf Oscillator on a Printed Circuit Board for Multipole Ion Guides. *Rev. Sci. Instrum.* **2006**, *77* (11). https://doi.org/10.1063/1.2387881.
(44) March, R. QUADRUPOLE ION TRAPS. *MASS Spectrom. Rev.* **2009**, *28* (6), 961–989. https://doi.org/10.1002/mas.20250.
(45) Douglas, D. LINEAR QUADRUPOLES IN MASS SPECTROMETRY. *MASS Spectrom. Rev.* **2009**, *28* (6), 937–960. https://doi.org/10.1002/mas.20249.
(46) Hoffman, N.; Opacic, B.; Reilly, P. Note: An Inexpensive Square Waveform Ion Funnel Driver. *Rev. Sci. Instrum.* **2017**, *88* (1), 016104. https://doi.org/10.1063/1.4974345.
(47) Hoffman, N.; Gotlib, Z.; Opacic, B.; Clowers, B.; Reilly, P. A Comparison Based Digital Waveform Generator for High Resolution Duty Cycle. *Rev. Sci. Instrum.* **2018**, *89* (8), 084101. https://doi.org/10.1063/1.5004798.

(48) Brabeck, G. F.; Reilly, P. T. A. Mapping Ion Stability in Digitally Driven Ion Traps and Guides. *Int. J. Mass Spectrom.* **2014**, *364*, 1–8. https://doi.org/10.1016/j.ijms.2014.03.008.
(49) Huntley, A.; Opacic, B.; Brabeck, G.; Reilly, P. Simulation of Instantaneous Changes in Ion Motion with Waveform Duty Cycle. *Int. J. MASS Spectrom.* **2019**, *441*, 8–13. https://doi.org/10.1016/j.ijms.2019.03.007.
(50) Opacic, B.; Huntley, A.; Clowers, B.; Reilly, P. Digital Mass Filter Analysis in Stability Zones A and B. *J. MASS Spectrom.* **2018**, *53* (12), 1155–1168. https://doi.org/10.1002/jms.4295.
(51) Bandelow, S.; Marx, G.; Schweikhard, L. The Stability Diagram of the Digital Ion Trap. *Int. J. MASS Spectrom.* **2013**, *336*, 47–52. https://doi.org/10.1016/j.ijms.2012.12.013.
(52) Huntley, A.; Reilly, P. New Tools for Theoretical Comparison of Rectangular and Sine Wave Operation of Ion Traps, Guides and Mass Filters. *J. MASS Spectrom.* **2020**, *55* (12), e4661. https://doi.org/10.1002/jms.4661.
(53) Gerlich, D. Inhomogeneous RF-Fields - A Versatile Tool for the Study of Processes with Slow Ions. *Adv. Chem. Phys.* **1992**, *82*, 1–176.
(54) Soni, M.; Cooks, R. Selective Injection and Isolation of Ion in Quadrupole Ion-Trap Mass-Spectrometry Using Notched Wave-Forms Created Using the Inverse Fourier-Transform. *Anal. Chem.* **1994**, *66* (15), 2488–2496. https://doi.org/10.1021/ac00087a013.
(55) McLuckey, S.; Goeringer, D.; Glish, G. Selective Ion Isolation Rejection over a Broad Mass Range in the Quadrupole Ion Trap. *J. Am. Soc. MASS Spectrom.* **1991**, *2* (1), 11–21. https://doi.org/10.1016/1044-0305(91)80056-D.

TOC graphic

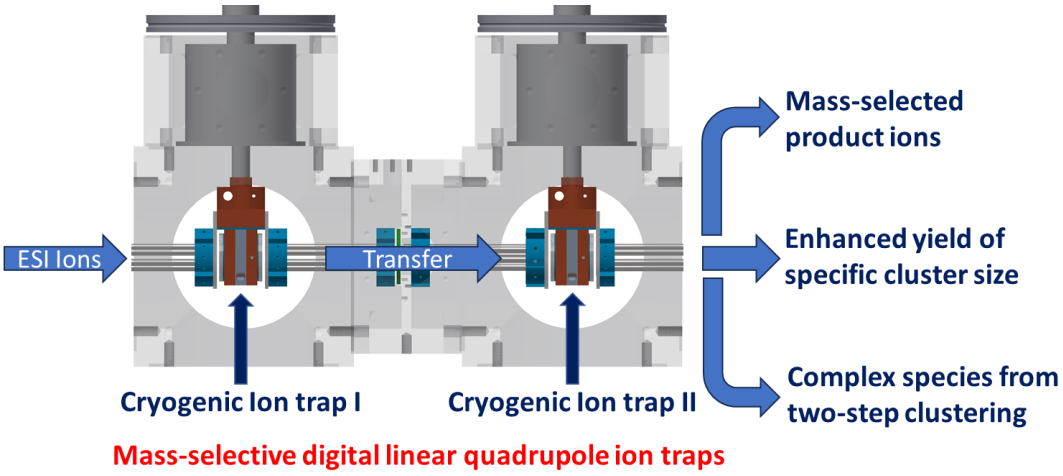
ESI Ions
Transfer
Cryogenic Ion trap I
Cryogenic Ion trap II
Mass-selected product ions
Enhanced yield of specific cluster size
Complex species from two-step clustering
Mass-selective digital linear quadrupole ion traps